**Proceedings of the ASME 2013 International Design Engineering Technical Conferences & Computers and Information in Engineering Conference**
**IDETC/CIE 2013**
**August 4-7, 2013, Portland, OR, USA**

**DETC2013-12348**

# ACCOMMODATING THICKNESS IN ORIGAMI-BASED DEPLOYABLE ARRAYS

**Shannon A. Zirbel**
**Spencer P. Magleby**
**Larry L. Howell***
Dept. of Mechanical Engineering
Brigham Young University
Provo, UT 84602

**Robert J. Lang**
Lang Origami
Alamo, CA 94507
*www.langorigami.com*

**Mark W. Thomson**
**Deborah A. Sigel**
**Phillip E. Walkemeyer**
**Brian P. Trease**
Jet Propulsion Laboratory
California Institute of Technology
Pasadena, CA 91109

## ABSTRACT

*The purpose of this work is to create deployment systems with a large ratio of stowed-to-deployed diameter. Deployment from a compact form to a final flat state can be achieved through origami-inspired folding of panels. There are many models capable of this motion when folded in a material with negligible thickness; however, when the application requires the folding of thick, rigid panels, attention must be paid to the effect of material thickness not only on the final folded state, but also during the folding motion (i.e., the panels must not be required to flex to attain the final folded form). The objective is to develop new methods for deployment from a compact folded form to a large circular array (or other final form). This paper describes a mathematical model for modifying the pattern to accommodate material thickness in the context of the design, modeling, and testing of a deployable system inspired by an origami six-sided flasher model. The model is demonstrated in hardware as a 1/20th scale prototype of a deployable solar array for space applications. The resulting prototype has a ratio of stowed-to-deployed diameter of 9.2 (or 1.25 m deployed outer diameter to 0.136 m stowed outer diameter).*

## INTRODUCTION

The purpose of this work is to develop deployment systems that unfold from a compact form to a large array. This work is motivated by the need for compactly folded solar arrays for space applications. A large ratio of stowed-to-deployed diameter enables large solar arrays to be launched in their compact, folded configuration and then deployed in space to a much larger surface area. For our objectives, a design with synchronous deployment was desired to simplify actuation and deployment.

Deployment from a compact form to a final flat state can be achieved through origami-inspired folding of panels. There are many models capable of this motion when folded in paper or other materials with negligible thickness; however, when the application requires the folding of thick, rigid panels, material thickness can inhibit the folding motion. To be rigid-foldable, the panels must not be required to flex to attain the final folded form.

This paper describes the approach for modifying the design of an origami six-sided flasher model to accommodate material thickness. This work builds on existing models to present a unique design that is rigid-foldable through two different methods. In the first method, the panels are allowed to flex along their diagonals. In the second method, the panels are affixed to a flexible membrane with discrete gap spacing between the panels. Both folding solutions enable the model to be rigid-foldable.

## BACKGROUND

Origami-inspired folding of deployable systems can enable a compactly stowed volume during launch and flight that will

*Corresponding author: lhowell@byu.edu


Copyright © 2013 by ASME

be deployed into a much larger volume when the target location is reached. Origami models are generally created for near zero thickness material. Panel thickness is one of the main challenges of origami-inspired engineering design. Rigid-foldable origami (also called rigid origami) defines those models that can still be folded when the facets are replaced with rigid panels and the creases are replaced with hinges [1]. The field of rigid-foldable origami is an active area of research and has many open problems.

Tachi has achieved rigid foldability with non-concurrent axes, where the axes are shifted to enable the model to fold, as shown in Figure 1a [2], or by reallocating material or removing material near the fold line, as shown in Figure 1b [2].

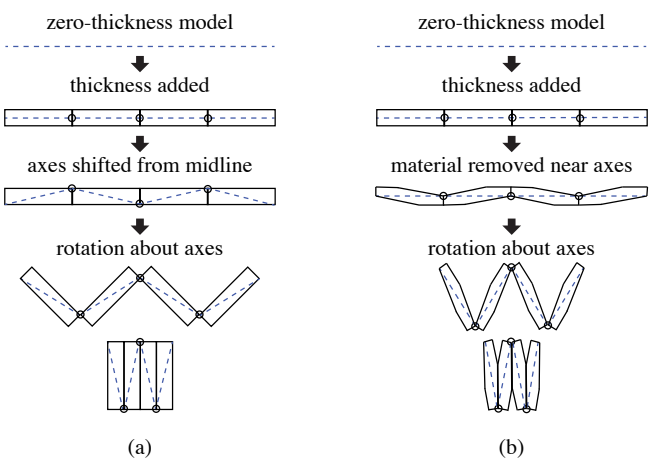


**FIGURE 1**. Two approaches for enabling origami with thickness, from Tachi [2]: (a) The axis of rotation for the fold is shifted from the midline of the material to the material surface. (b) Material is removed near the fold line. In both (a) and (b), the dashed line represents the zero-thickness model.

Trautz and Künstler [3] identified the hinge translations that occur when thickness is added to the model. Without other compensation, a degree-4 vertex (or a spherical mechanism) with thickness added must allow sliding along the rotational axes or hinge lines to compensate for the doubled number of constraints around each vertex and to enable the model to fold.

Hinge components are often added to the model to enable the folding of thick, rigid materials. Hoberman [4–6] has presented several concepts related to adding hinges to thick rigid origami to enable foldability. In his earlier work, tapered strips accounted for material thickness and ordered pleating enabled the thick sheets to collapse on themselves. In more recent work, the hinges do not lie in the same plane, so their axes do not intersect [6]. These offsets enable the mechanism to be rigid-foldable into a compact unit. Hoberman mechanisms were used by Faist and Wiens in 2010 in the design of deployable antennae and solar arrays [7].

The Miura-ori model is one of the landmark rigid-foldable deployable structures [8, 9]. The Miura-ori fold pattern is folded like a map fold, but with angled folds along one dimension (see Figure 2). The resulting package is mostly synchronous, but has a slight lateral offset. As the angle increases, the package opens more synchronously (with $x$ and $y$ opening almost at the same time). As the angle decreases, the package opens with less synchrony. The trivial 0 degree case is the map-fold, where the model unfolds entirely in one direction before the perpendicular direction can unfold.

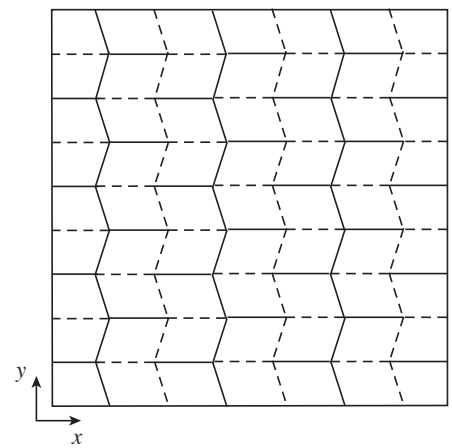


**FIGURE 2**. Crease pattern for the Miura-ori fold, based on [8, 9].

Sternberg [10] presented several concepts showing collapsible folds in origami. He briefly addresses the problem of material thickness, but he particularly addresses the problem of collapsibility (or conversely, deployability). He suggests that introducing slight asymmetry to the model allows the collapse to occur. While the symmetry provides the rigidity in the model, a slight skew in the pattern will allow compressive and tensile forces to be "released", thus enabling the model to collapse.

Guest and Pellegrino [11] presented a modeling technique for wrapping thin membranes around a central hub. They showed that the model can be adjusted for thickness by increasing the panel dimensions as the distance from the center of the model increases and that the six-sided flasher model can be "inextensional" (i.e., the panels are unstretched) in its flat and folded states, but not necessarily in transition between the two.

Nojima [12] also presented several radially deployable origami models, many of which are generalizations of the Guest/Pellegrino winding membrane structure and are related


Copyright © 2013 by ASME

closely to the model used in this work. Guest and De Focatiis also published work on deployable membranes which were achieved by combining several corrugated patterns [13].

The patterns described by Guest and Pellegrino [11] and Nojima [12] allow the folding of an arbitrarily large, roughly circular region into a polygonal cylinder (or cone, as in some of Nojima's structures), whose diameter in the folded form is much smaller than that of the unfolded surface. A notable property of these structures is that for a given central polygon diameter, the diameter of the folded cylinder stays roughly fixed as the diameter is increased, while the length of the cylinder increases roughly linearly with the diameter of the unfolded pattern. This scaling factor can be reduced by increasing the rotational order of symmetry of the pattern, or increasing the number of sides of the central polygon.

This "winding membrane" family of patterns has been independently (re)discovered many times by researchers and artists alike. Within the world of origami, Shafer and Palmer, inspired by unpublished work of David Huffman (personal communication, ca. 2005), developed a concept that has come to be called a "flasher" [14–16]. A notable innovation of the Shafer/Palmer flasher was the addition of multiple folds along mirror planes normal to the cylindrical axis, which allows the structure to maintain roughly constant diameter *and* roughly constant cylindrical length as the diameter of the unfolded pattern increases, albeit at the cost of a now quadratic, rather than linear, increase in the number of layers wrapping around the cylinder. This property of roughly constant size as the unfolded diameter is scaled makes the "flasher" family of structures particularly suitable for deployable structures, and it is the basis of the structure we investigate in the present work.

## MATHEMATICAL MODEL

The most common mathematical models of origami assume zero thickness for the paper, so that when layers of paper are stacked, they are (mathematically) coplanar. When a material with finite thickness is used, the panels analogous to the paper layers are not coplanar; they must stack with finite spacing, and this behavior forces a folded structure to differ in several ways from its zero-thickness idealization.

The process of adding thickness to the mathematical model qualitatively changes the folding action. Mechanisms that are possible with zero thickness may not be possible with finite thickness. Notably, with a zero-thickness model, the degree-4 vertex has a single degree of freedom; it is a spherical four-bar linkage [17]. If, however, one creates such a vertex with thick panels by placing hinges on the top and bottom surfaces of the panels (corresponding to valley and mountain folds, respectively), then it no longer necessarily has a single degree of freedom; in general, additional translational motion along hinges, or the equivalent, may be required to preserve the single-DOF motion, as noted by Künstler and Trautz [3].

However, Tachi has demonstrated [1] a method of creating a 3D structure with panels of finite thickness that has the same kinematic behavior as the zero-thickness model by effectively embedding a zero-thickness mechanism within a set of thick panels. Such a mechanism flexes in the same way as the original zero-thickness model. However, for this approach to be applied, a necessary condition is that the fully folded state cannot have coplanar facets; rather, the facets must be separated by finite distance and/or nonzero angular separation in the fully folded state to leave room for the thickness of the panels.

Similarly, the zero-thickness model of the fully unfolded state of such a structure is not truly flat; it is slightly folded and embedded within thick panels in such a way that the panel surfaces are flat even though the zero-thickness surface is not.

Such zero-thickness models of origami that incorporate finite spacing between layers can serve as tools for design and can provide desirable motions of deployment. They are a useful intermediate step between a fully flat, zero-thickness model and a true 3D model that fully incorporates thickness. We call a zero-thickness model that incorporates finite distance and/or angular separation between contacting layers a *thickness-accommodating* model of origami. Thickness-accommodating models can be useful directly, by applying a thickening algorithm such as those proposed by Tachi [1], and also as an approximation of a fully 3D structure that has greater fidelity than a flat zero-thickness model.

In a theoretical zero-thickness winding-membrane structure, all of the cylindrically wrapped layers are coplanar with their neighbors. In a physical structure, the layers must be slightly separated from one another to accommodate the thickness of the individual panels. A winding-membrane deployable could be realized based on a thickness-accommodating model in which the wrapped layers are logarithmically separated from one another radially, rather than coplanar, in the fully folded state. This type of modification was noted by Guest and Pellegrino [11]. Such modification of the crease pattern gives rise to a slight apparent curvature (a piecewise linear curve) in some of the folding lines of the unfolded pattern, as shown in Figure 3 [11]. A similar curvature is required in a thickness-accommodating flasher, shown in Figure 4.

Creating a thickness-accommodating mathematical model of a flasher is somewhat more complicated, because the number of layer thicknesses must increase quadratically with the diameter of the unfolded pattern to keep a constant separation between consecutive layers in the wrapping pattern. Because of this quadratic factor, there is no simple formula for the vertices of a thickness-accommodating flasher pattern. Nevertheless, we can construct a numerical solution in a straightforward fashion, and because this method is applicable to a wide range of origami structures, we describe it in some detail in the following section.


Copyright © 2013 by ASME

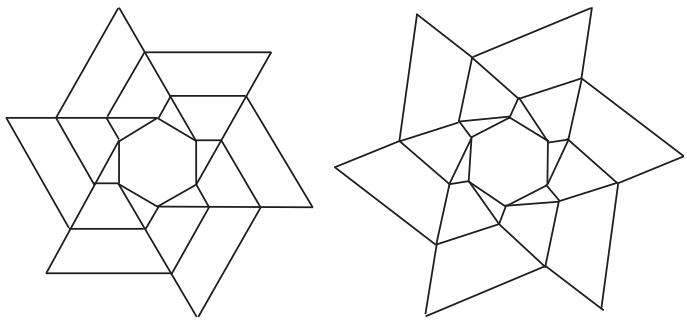

(a) (b)

**FIGURE 3**. Comparison of (a) ideal and (b) thickness-accommodating winding membrane from Guest and Pellegrino [11].

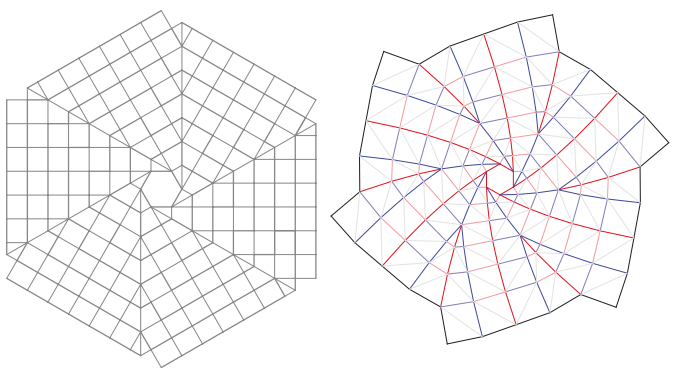

(a) (b)

**FIGURE 4**. The six-sided flasher model. (a) Model assuming zero-thickness (b) Crease pattern for the model assuming finite thickness, with additional diagonal folds included to enable rigid-foldability.

## Mathematical Model: Development

The basic design approach for a thickness-accommodating flasher is relatively straightforward. We describe both the crease pattern and the folded form by the coordinates of their vertices (2D vectors for the crease pattern, 3D vectors for the folded form), then apply two sets of constraints:

1. Constraints that specify the desired shape of the crease pattern and folded form;
2. Constraints that enforce *isometry* between the crease pattern and folded form.

The isometry constraints ensure that the folded form is a piecewise isometric (inextensional) transformation of the crease pattern, meaning that for any two points connected by a straight line within the surface in both crease pattern and folded form, their separation distances must be the same. We note, though, that the existence of isometry between the crease pattern and folded form does not ensure the existence of a rigidly foldable transformation from one to the other, one in which no facet stretches, compresses, or bends. However, in practice, physical models of such structures do typically have a smooth transformation between states (in some cases, a quite spectacular smooth transformation), which suggests that non-rigid deformations, if necessary (such as described by Trautz and Künstler [3]), may be sufficiently small that they could be provided by local compliance in the folding structure and/or small further modification of the folding pattern.

The radial symmetry of flashers allows for some simplification in their analysis; one need not solve for all of the vertex coordinates independently. It is sufficient to solve for the coordinates of a single sector and then use rotational symmetry to construct the full pattern.

In general, a flasher crease pattern will consist of a central polygon that we take to be a regular unit polygon with $m$ sides; we call $m$ the *rotational order* of the flasher. The crease pattern consists of a set of panels in $m$ geometrically similar sectors around the central polygon. In the folded form, each sector folds into a set of partial rings that wrap cylindrically around the central polygon and each other so that the layers are (ideally) evenly spaced from one another as one moves out from the central polygon. In each sector, most panels are rectangular, but a subset are triangular; the triangles are created by a prominent chain of diagonal folds, one in each sector, that begins at the central polygon, then sequentially rises and falls as it wraps around the cylinder.

We can characterize a wide variety of flashers by a small number of parameters. In addition to $m$, the rotational order, we define integer $h \geq 1$ as the *height order*, which is the number of axial bends it takes for the diagonal fold to travel once from the bottom to the top of the cylinder in the folded form. In Figure 5, $h = 2$ because of the two segments $\mathbf{p}_{0,0,-1}$–$\mathbf{p}_{0,1,0}$ and $\mathbf{p}_{0,1,0}$–$\mathbf{p}_{1,2,0}$.

We define $r \geq 1$ as the number of distinct "rings" in the pattern, or equivalently (and more precisely), the number of times the diagonal moves from bottom to top and vice-versa. In Figure 5, $r = 2$ because the segment $\mathbf{p}_{0,0,-1}$–$\mathbf{p}_{0,1,0}$ moves from bottom to top and segment $\mathbf{p}_{1,2,0}$–$\mathbf{p}_{2,3,0}$ moves from top to bottom. For comparison, in Figure 4b, $m = 6$, $h = 3$, and $r = 2$.

We now set up a coordinate system of indexed points $\mathbf{p}_{i,j,k}$ for points in the crease pattern and $\mathbf{p}'_{i,j,k}$ as their respective images in the folded form, with indices defined as follows. Each sector consists of two parts, divided by the diagonal chain of creases. For point $\mathbf{p}_{i,j,k}$, in the larger portion of the sector (on the left in Figure 5), index $i \geq 0$ increases as one moves out along a crease incident to the central polygon whose folded form lies (approximately) in the $xy$ plane, with $i = 0$ being a corner of the central polygon. Index $j \geq 0$ takes on the value 0 along that same crease, then increases as one moves perpendicularly to this crease within the crease pattern. In the smaller portion of the sector, as one moves away from the central polygon (along lines that are roughly the diagonal reflection of lines of constant $j$ in the larger part) $i$ stays fixed and $j$ increases sequentially. This numbering


Copyright © 2013 by ASME

scheme gives a unique $(i, j)$ pair to every point within a single sector.

Index $k$ specifies the rotational sector that the point belongs to, and so because of the rotational symmetry of order $m$, we will have

$$\mathbf{p}_{i,j,k} \equiv \mathbf{p}_{i,j,k+m}, \mathbf{p}'_{i,j,k} \equiv \mathbf{p}'_{i,j,k+m}. \tag{1}$$

A single sector for $m = 6$, $h = 2$, $r = 2$ is shown in Figure 5 for both the crease pattern and the folded form.

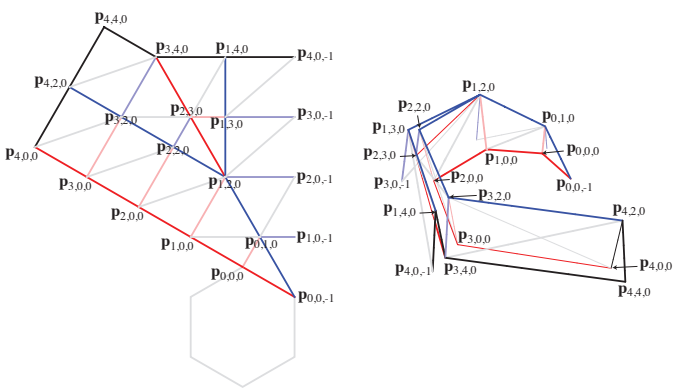


**FIGURE 5**. A single labeled sector of crease pattern (left) and folded form (right), showing how the vertices are indexed. In the crease pattern, the central polygon is outlined in light gray. For this sector, $m = 6$, $h = 2$, and $r = 2$.

Note that in general, $j$ runs from 0 to $r \times h$, but for $h > 1$ (as in this example, $h = 2$), there are not vertices for all values of $(i, j, k)$. In particular, for most values of $i$, index $j$ only takes on values that are multiples of $h$ except along the diagonal crease, where there is a vertex for each value of $j$ up to $j = r \times h$.

In these figures, we have colored fold lines according to their fold direction. Red lines are valley folds (with positive fold angle); blue lines are mountain folds (negative fold angle). Fold lines can be further characterized as *sharp*, if the fold angle is (nearly) equal to $\pm 180°$, *medium* if it is generally between $\pm 180°$ and $0°$, and *slight*, if it is nearly equal to $0°$. We draw medium mountain and valley folds in a lighter shade of red or blue, respectively; slight folds will be drawn in light gray, irrespective of their actual fold direction.

In general, the values of the coordinates in both the 2D crease pattern and 3D folded form are to be solved for. It is useful, though, to have a set of approximate coordinate values, which can be used as starting values for a numerical optimization.

**Zero-thickness flasher model** For an ideal zero-thickness, non-thickness-accommodating flasher, the 2D and 3D coordinates are given as follows.

For convenience, we define the unit vector

$$\mathbf{u}(\theta) \equiv (\cos\theta, \sin\theta), \tag{2}$$

and the 2D rotation matrix in the usual way,

$$\mathbf{R}(k) \equiv \begin{pmatrix} \cos\frac{2\pi k}{m} & -\sin\frac{2\pi k}{m} \\ \sin\frac{2\pi k}{m} & \cos\frac{2\pi k}{m} \end{pmatrix}. \tag{3}$$

The 2D crease pattern points are given by

$$\mathbf{p}_{i,j,k} = \mathbf{R}(k) \cdot \left[ \frac{1}{2}(\cot\frac{\pi}{m}, 1) + \begin{cases} (i+1)\mathbf{u}(\frac{\pi}{2} + \frac{2\pi}{m}) + (j)\tan\frac{\pi}{m}\mathbf{u}(\frac{2\pi}{m}) & \text{if } i+1 \geq j \\ (j)\mathbf{u}(\frac{\pi}{2}) - (i+1)\tan(\frac{\pi}{m})\mathbf{u}(0) & \text{otherwise} \end{cases} \right] \tag{4}$$

To compute the 3D folded form points, it is helpful to define some auxiliary functions. We define $\mathrm{rot}(i, j)$ as the number of angular increments (of $2\pi/m$) that the point $\mathbf{p}'_{i,j,k}$ gets rotated relative to $\mathbf{p}'_{0,0,k}$ (which is the $k$th corner of the central polygon). Its value is given by

$$\mathrm{rot}(i, j) \equiv \begin{cases} i+1 & \text{if } j \leq i+1 \\ j & \text{otherwise} \end{cases}. \tag{5}$$

We define $\mathrm{ht}(i, j)$ as the discrete (normalized) height of $\mathbf{p}'_{i,j,k}$ above the $xy$ plane. It is given by

$$\mathrm{ht}(i, j) \equiv |(\min(i+1, j) - h) \bmod 2h) - h|. \tag{6}$$

We also define the 3D rotation matrix

$$\mathbf{R}'(k) \equiv \begin{pmatrix} \cos\frac{2\pi k}{m} & \sin\frac{2\pi k}{m} & 0 \\ \sin\frac{2\pi k}{m} & \cos\frac{2\pi k}{m} & 0 \\ 0 & 0 & 1 \end{pmatrix}. \tag{7}$$

Then the zero-thickness, non-thickness-accommodating folded form point $\mathbf{p}'_{i,j,k}$ has the value

$$\mathbf{p}'_{i,j,k} = \mathbf{R}'(k + \mathrm{rot}(i, j)) \cdot \left[ \frac{1}{2}(\cot\frac{\pi}{m}, 1, 0) + (0, 0, \mathrm{ht}(i, j)\tan\frac{\pi}{m}) \right]. \tag{8}$$

These are, in fact, exact values for the zero-thickness, non-thickness-accommodating case (shown in Figure 4a); the resulting crease patterns and folded forms are isometries of one another, but all of the layers in each wall of the cylinder are coplanar.


Copyright © 2013 by ASME

**Thickness-accommodating flasher model** To accommodate thickness, we would like to add spacing between layers moving out radially from the central polygon. Because a panel is defined by its vertices, we need to space out vertices that are physically adjacent. To do this, we need a radial ordering function for vertices that gives their stacking order.

We define a new auxiliary function $\mathrm{rad}(i,j) = 0,1,2,\ldots$ that is a discrete radial spacing function that describes the radial ordering of the vertices of successive layers as they wind around the central polygon. We want to assign each vertex to a distinct and unique radial "slot" (for a given rotational position $k$) so that no two vertices have the same position and the relative ordering of all of the vertices is such that there is no self-intersection of any panels as they wrap around. A formula for $\mathrm{rad}(i,j)$ that satisfies these requirements is

$$\mathrm{rad}(i,j) \equiv \begin{cases} i(i+1)+j & \text{if } j \le i+1 \\ j(j+1)-(i+1) & \text{otherwise} \end{cases}. \tag{9}$$

The function $\mathrm{rad}(i,j)$ is a discrete, integer-valued function that maps each point to a radial ordering. We now introduce a floating-point value, $\delta$, which is the desired separation between two nearest-neighbor vertices at the same radial position and the same $z$ coordinate, normalized to the diameter of the circumcircle of the central polygon. That is, if the diameter of the circumcircle is $d$, then we want any two vertices that are adjacent at the same $z$-height to be spaced by a distance $\delta d$. Spreading out the layers radially (without changing the $z$-values of their coordinates) gives the modified coordinate values

$$\mathbf{p}'_{i,j,k} = \mathbf{R}'(k+\mathrm{rot}(i,j)) \cdot \left[\frac{1}{2}(1+\frac{\delta}{h}\mathrm{rad}(i,j))(\cot\frac{\pi}{m},1,0) + (0,0,\mathrm{ht}(i,j)\tan\frac{\pi}{m})\right]. \tag{10}$$

We have used this formula for the 3D vertex coordinates in Figure 5 with $\delta = 0.2$, which results in a separation between vertex coordinates that would otherwise overlap.

Equation (10) gives coordinate values that provide the desired separation between layers. However, the folded form implied by this equation is no longer an isometry of the crease pattern implied by Equation (4). In fact, it will in general not even unfold to a flat shape. The challenge, therefore, is to find a set of crease pattern and folded form coordinates where the former is flat, the latter has spacing between adjacent layers, and each is an isometry of the other.

## Mathematical Model: Optimization

The optimization routine defines the set of points that satisfy the shape and isometry constraints. More specifically, our approach for solving for the thickness-accommodating flasher pattern is to pin some of the coordinate values $\{\mathbf{p}_{i,j,k}, \mathbf{p}'_{i,j,k}\}$ to the values given by Equations (4) and (10) to define the desired shape and layer spacing and to let others vary so that we can satisfy the isometry conditions.

We define the coordinate values given by Equations (4) and (10) as $\mathbf{p}^{(0)}_{i,j,k}$ and $\mathbf{p}'^{(0)}_{i,j,k}$, respectively. We then define each of the variable vertex vectors by its scalar coordinates (identified by an additional subscript), e.g.,

$$\mathbf{p}_{i,j,k} \equiv (p_{i,j,k,x}, p_{i,j,k,y}), \tag{11}$$

and similarly for the folded form,

$$\mathbf{p}'_{i,j,k} \equiv (p'_{i,j,k,x}, p'_{i,j,k,y}, p'_{i,j,k,z}). \tag{12}$$

Then we can enforce the overall shape of the folded form and the explicit separation between wrapped layers by requiring that the $x$- and $y$-coordinates take on their ideal values,

$$p'_{i,j,k,x} = p'^{(0)}_{i,j,k,x},\ p'_{i,j,k,y} = p'^{(0)}_{i,j,k,y}, \tag{13}$$

but we will allow the $z$-coordinate, $p'^{(0)}_{i,j,k,z}$ to be a variable to be solved for.

In the crease pattern, we allow both scalar components of the vector coordinates to be variables. Thus, if there are $N$ vertices in the flasher pattern, we fix $2N$ of the $5N$ vertex coordinates and allow the other $3N$ to be variables that we will solve for.

Of course, we only need to solve for the variables in a single sector ($k = 0$); all of the others can be computed by suitable rotations of the initial sector.

To remove rotational ambiguity in the crease pattern, we can fully fix the corner of the central polygon:

$$\mathbf{p}_{0,0,0} = \mathbf{p}^{(0)}_{0,0,0} = \frac{1}{2}(\cot\frac{\pi}{m},1). \tag{14}$$

Similarly, in the folded form, we can fix the $z$-coordinate of the central polygon to 0 (in addition to the $x$- and $y$-coordinates, which we have already fixed).

Now we turn our attention to isometry. The folded form must be an isometric transformation of the crease pattern. This means that for any two vertices connected by a folded edge, the length of the fold must be the same in the crease pattern and folded form. This is the *isometry condition* on a vertex pair: if $\mathbf{p}_{i,j,k}$ and $\mathbf{p}_{l,m,n}$ are two vertices connected by a folded edge, we must have

$$|\mathbf{p}_{i,j,k} - \mathbf{p}_{l,m,n}| = |\mathbf{p}'_{i,j,k} - \mathbf{p}'_{l,m,n}|. \tag{15}$$


Copyright © 2013 by ASME

This gives an equation constraint for every folded edge in the crease pattern, but by making use of rotational symmetry, we need only consider the set of such constraints for every folded edge in a single sector of the pattern.

The isometry conditions for folded edges are necessary to ensure overall isometry, but they are not necessarily sufficient. For triangular facets (panels), if the vertices are pairwise isometric, then the three vertices define a unique isometric mapping from the crease pattern to the folded form. For a quadrilateral, however, an additional condition is required to ensure existence of an isometric transformation: at least one of the diagonals must also be isometric. If the quadrilateral is planar, then both diagonals will be isometric.

As we have defined the pattern thus far, the quadrilaterals are not necessarily planar, and so even if the crease-pattern-to-folded-form mapping is piecewise isometric, only one of the diagonals will, in general, be isometric—but we must force one of them to isometry. We have the freedom to choose which one is forced to isometry for each panel. There is a physical interpretation of this choice; if a quadrilateral is nonplanar, then the diagonal that is isometric is a slight fold in the panel along the line of isometry. We have shown such folds (and our choice of diagonal) as a light gray line in the plot. As noted earlier, even with an isometric map between the crease pattern and folded form, there is no guarantee of a rigidly foldable path from one to the other; we conjecture, though, that the addition of such diagonal folds gives sufficient flexibility for rigid foldability. (We further conjecture that the necessary amount of flexing along these diagonals is always slight, so that such folds may be made much stiffer than the primary folds in the pattern.)

Whatever the degree to which a pattern flexes along quadrilateral diagonals, it is necessary to enforce isometry on one diagonal of each quadrilateral, and so this requirement creates another set of equation constraints on the system of variables: in this case, one more isometry for each quadrilateral in the crease pattern.

The constraints described thus far—fixing of coordinate values in the crease pattern and folded form, isometry conditions on folded edges and quadrilateral diagonals—do not yet add up to the $5N$ degrees of freedom in the system of $N$ vertices within a sector. In fact, a careful enumeration reveals that for the flasher family $\{m,h,r\}$, there remain $2r$ available degrees of freedom. We can use these to specify some, though not all, of the $z$-coordinates in the folded form.

Specifically, we choose the $z$-coordinates of the vertices on the outside edge of the pattern (the vertices on the black boundary lines in Figure 5). We would like to choose these values so that as one moves around the edge, the vertices take on $z$-coordinate values close to their zero-thickness, non-thickness-accommodating values, i.e., they alternate between "up" and "down" values, giving the desired fan-fold structure at the outside edge.

We have $2r$ degrees of freedom, but there are $2r+1$ coordinate values to set on the boundary of a sector. Rather than arbitrarily leaving out one vertex, we introduce a new slack variable $\zeta$, which we define as an overall scaling factor, which gives us the necessary additional degree of freedom. So for each of the $2r+1$ folded form vertices $\mathbf{p}'_{i,j,0}$ on the boundary of sector $k=0$, we impose the condition

$$p'_{i,j,0,z} = \zeta p'^{(0)}_{i,j,0,z}, \tag{16}$$

and the new variable $\zeta$ gives us the necessary additional degree of freedom in the system.

With this variable introduction, we achieve precise equality between the number of variables and number of constraints; the problem is fully defined. The various constraint equations are algebraic and nonlinear; such systems are readily amenable to computer numerical solution.

We have created a Mathematica 8 notebook that sets up the constraints for a general flasher and solves for vertex coordinates for both the crease pattern and folded form. (It is available for download [18].) Figure 6 shows several wire-frame views of the crease pattern and folded form for $m=6$, $h=2$, $r=2$, and $\delta=0.1$. We have used this notebook to solve for several thickness-accommodating flasher patterns and have built and tested physical models of several, as described next.

## PHYSICAL MODEL

The mathematical model defines the panel and hinge geometry that accommodates thickness in the folded configuration. Additional practical modifications are required to fabricate and test physical instantiations of the deployable system.

In this work, we explored two options for creating the rigid-foldable origami model: (1) allow the panels to fold along their diagonals (i.e. the model is entirely triangulated), or (2) apply a membrane backing to the entire model with specified widths at the fold-lines. Option (1) is the result of the mathematical model described above. Option (2) is motivated by the desire to keep the panels as large as possible to maximize the surface area to which solar cells may be affixed.

Option (1) allows the panels to fold along their diagonals, shown in grey in Figure 4b. These additional folds concentrate the "flexing" that occurs in the panels during the folding process to be along these new hinge lines. The rotation at the diagonals is less than 5 degrees, if all sides are actuated (folded) simultaneously.

The model is highly over-constrained. This can be seen in the Grübler-Kutzbach mobility equation for spatial mechanisms, which yields -36 degrees of freedom for the model shown in Figure 7.

Option (2) requires finding the optimal gap size to enable rigid foldability while maximizing panel surface area, shown


Copyright © 2013 by ASME

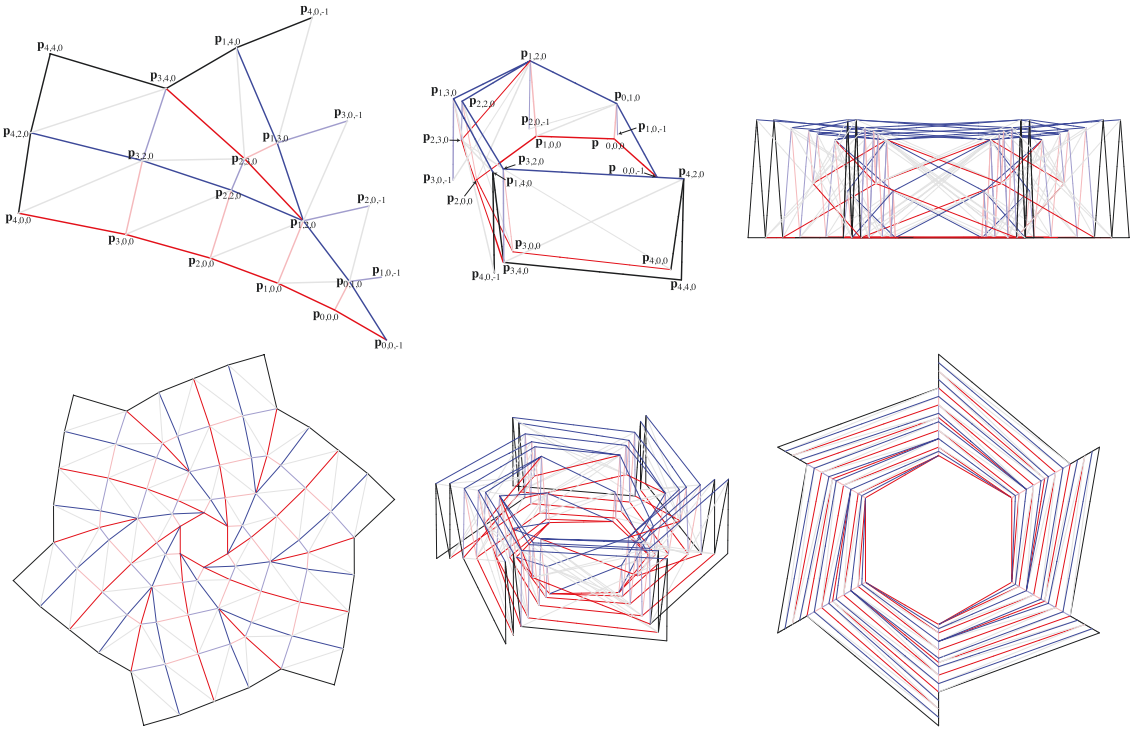

**FIGURE 6**. A thickness-accommodating flasher ($m = 6, h = 2, r = 2, \delta = 0.1$). Top row, l–r: crease pattern, single sector; folded form, single sector; folded form, side view. Bottom row, l–r: full crease pattern; full folded form; top view, folded form.

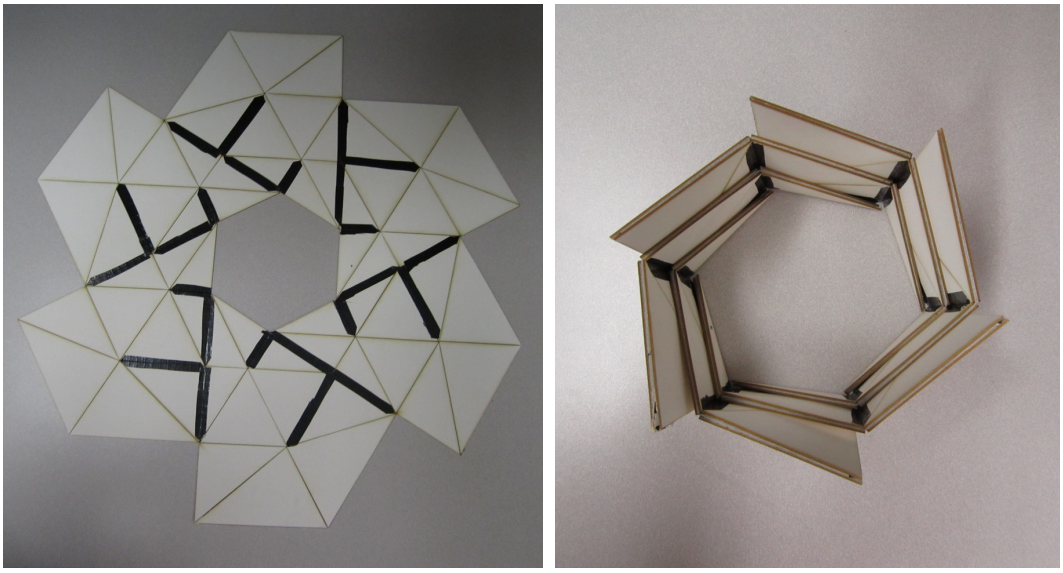

(a) (b)

**FIGURE 7**. The six-sided flasher ($m = 6$, $h = 3$, $r = 1$) is rigid-foldable when additional fold-lines are added to the model along the diagonals of each panel. (a) The model in its deployed configuration. (b) The model in its stowed configuration.


Copyright © 2013 by ASME

in Figure 8. The membrane simulates the folding of near-zero thickness material, but with extra material allowances given in the gaps between the thick rigid panels to make up for the thickness of the panels.

For the membrane model, the minimum spacing on valley folds undergoing 180 degrees of rotation is twice the thickness of the panels (Figure 9), as the membrane is applied to one side of the model only. The secondary valley folds undergo 60 degrees of rotation, and therefore could have a minimum spacing of one times the thickness (see Figure 9c).

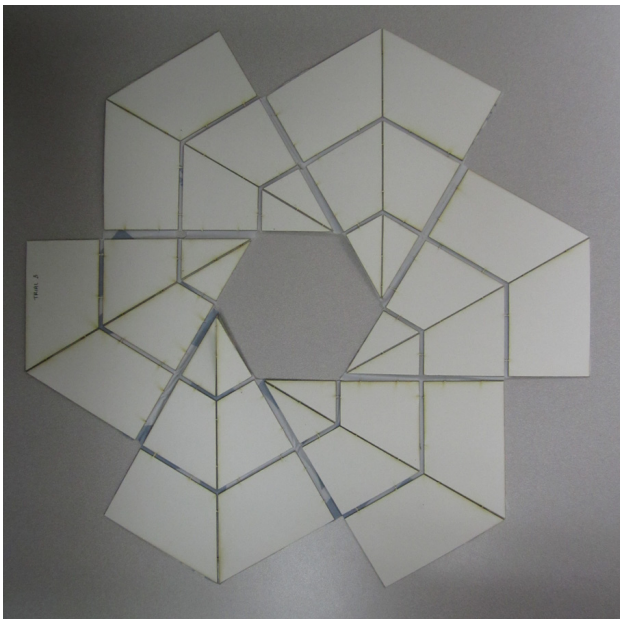

**FIGURE 8**. The gap width was adjusted at fold-lines to enable rigid folding of the model on a membrane backing. In this model, $m = 6$, $h = 3$, and $r = 1$.

The flasher model can be adjusted for materials of different thicknesses. Figure 10 shows the prototype in 2.5 mm thick balsa wood. The rigid panels were joined with an adhesive membrane on the side of the fold-line corresponding to the direction of the fold (mountain or valley). A gap was given in the valley folds (shown in Figure 10b) to enable the model to fold without requiring the panels to flex. Figures 10a and 10c show that the thickness of the one side of the stowed structure is equal to the combined thickness of the panels following the path outlined in orange; i.e., the number of panels along the orange path governs the thickness of the stowed structure.

## APPLICATION

Under NASA Technology Roadmaps, Flexible Material Systems refers to the "identification of flexible systems that enable the assembly of expandable structures from a small volume to a larger volume through the combined use of rigid linkages and joints with soft thin shells or membranes" [19]. A NASA Research Announcement [20] called for a mass and volume efficient solar array system. A large compression ratio of stowed-to-deployed diameter is needed to achieve the power requirement of 250 kW or greater. Origami folding patterns were used to inspire the folding of the solar array to achieve synchronous deployment.

The design constraints for the deployable solar array are:

1. Initial power levels of 30-50 kW, with extensibility to 250 kW for future applications;
2. Stowed dimensions to fit in launch vehicle;
3. Synchronous deployment preferable.

For comparison, the International Space Station has 8 solar arrays, generating 84 kilowatts of energy [21].

The flasher model [16] shows great promise as a large solar array deployer. It can be stowed around the circumference of a hexagonal spacecraft and deployed with a perimeter truss.

In the final model for the solar array, a membrane backing was selected to join the panels together. This was used together with the model designed to account for thickness. It necessitated the addition of gaps between the panels to enable rigid foldability. The model also required folding to occur in the membrane joints themselves, to preclude the solar panels from flexing. Therefore, the valley folds were given a gap width of 10 to 14 times the thickness of the panels. Mountain folds were given minimal separation to maximize the surface area of the panel.

The crease pattern was distorted using the algorithm described previously. In addition to the design constraints listed above, the following shape constraints were applied:

1. Hexagonal cross section ($m = 6$)
2. Maximum height of folded form = 4.0 m
3. Crease pattern incircle = 25.5 m
4. Maximum diameter (circumcircle) of folded form = 4.25 m
5. Maximum width of any panel = 2.0 m
6. Maximum spacing of any two vertices = (1 cm)sec(30°)

The mathematical model generated a thickness-accommodating pattern with $m = 6$, $h = 4$, $r = 2$, and $\delta = 0.01$.

A 1/20th scale model of the six-sided flasher is shown in Figure 11. It was built using Garolite (0.020" thick) and Kapton film for the backing (0.001" thick). The outer diameter is 1.25 meters. Gap spacing was included in the prototype to enable rigid foldability. Mountain folds require no gap. Valley folds are given more than the minimum 2x spacing to enable the panels to rotate away from each other during stow/deployment. The 1/20th scale prototype has gaps that are 14 times the panel thickness at


Copyright © 2013 by ASME

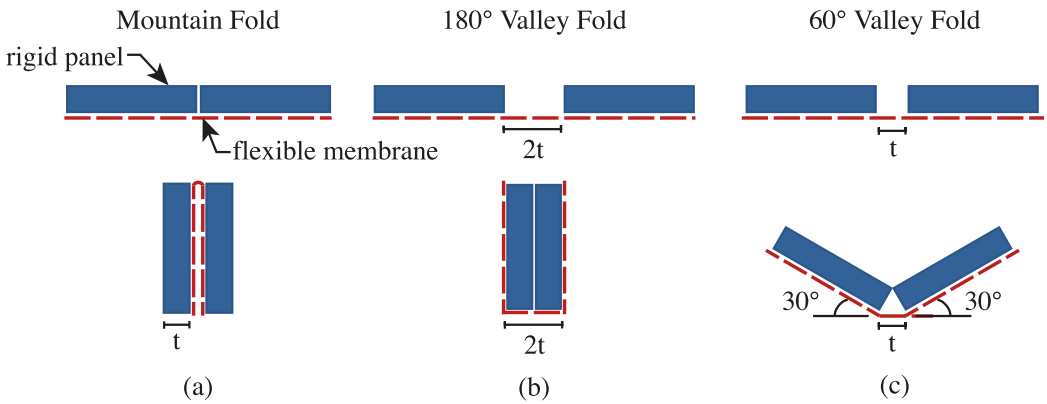


**FIGURE 9**. The folds of the membrane model are illustrated with the panels in blue and the membrane as the dashed red line. (a) The 180 degree mountain folds require minimal gap between panels because the membrane folds back on itself. (b) The 180 degree valley folds require a minimum of twice the thickness of the panels because the membrane folds around two panels. (c) The 60 degree valley folds require a minimum of one thickness because of the triangle formed by the panel edges.

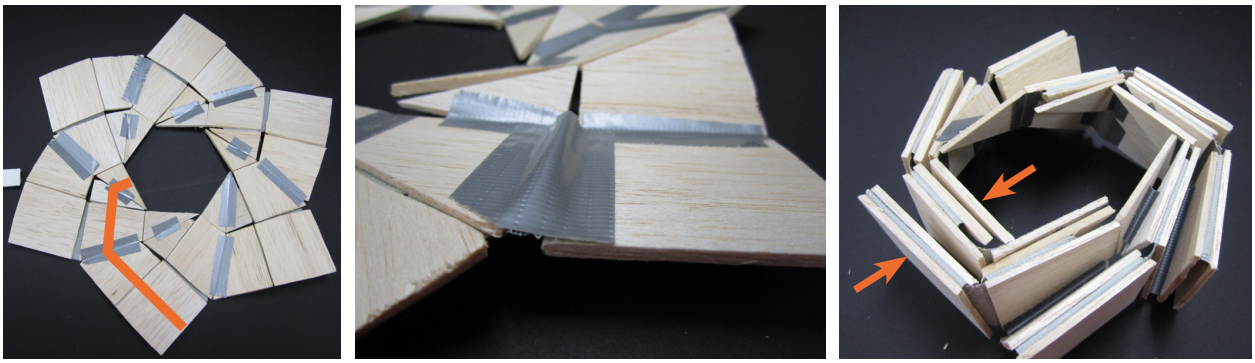


**FIGURE 10**. A rigid-foldable six-sided flasher ($m = 6$, $h = 2$, $r = 1$). The thickness of the panels governs the final size of the stowed model. (a) Deployed configuration; the orange path marks the number of panels on each side of the stowed model. (b) The rigid panels are hinged with an adhesive membrane on the side corresponding to the direction of the fold (mountain or valley). (c) Stowed configuration.

the 180 degree valley folds, and 10 times the panel thickness at 60 degree valley folds. Optimization based on the kinematics of folding may enable the gap spacing to be further reduced. The gap spacing may also be constrained by panel width and height, i.e., a larger panel may necessitate a wider gap to allow sufficient shear in the membrane.

The model has a stowed-to-deployed diameter ratio of 9.2 (or 1.25 m deployed diameter to 0.136 m stowed diameter). This ratio will increase as rows of panels are added to the circumference of the model.

## CONCLUSION

The origami flasher model inspired the development of a deployment system with a large ratio of stowed-to-deployed diameter. The pattern was modified for thick materials. By employing the mathematical model presented here, similar modifications can be made to other zero-thickness models to enable their rigid-foldability from thick materials.

The six-sided flasher has great promise as a large deployable array. However, there are still many unanswered questions regarding the joints and general assembly of the rigid flasher. By introducing the additional hinges along the diagonals (making all panels into triangles), the flasher model is rigid foldable. However, the additional folds increase the total degrees of freedom of the array. The ideal model would have exactly enough folds to result in a single-DOF mechanism. Loss of surface area coincident with option (1) makes it unfavorable for the solar array application. For this and other applications where that panel sub-


Copyright © 2013 by ASME

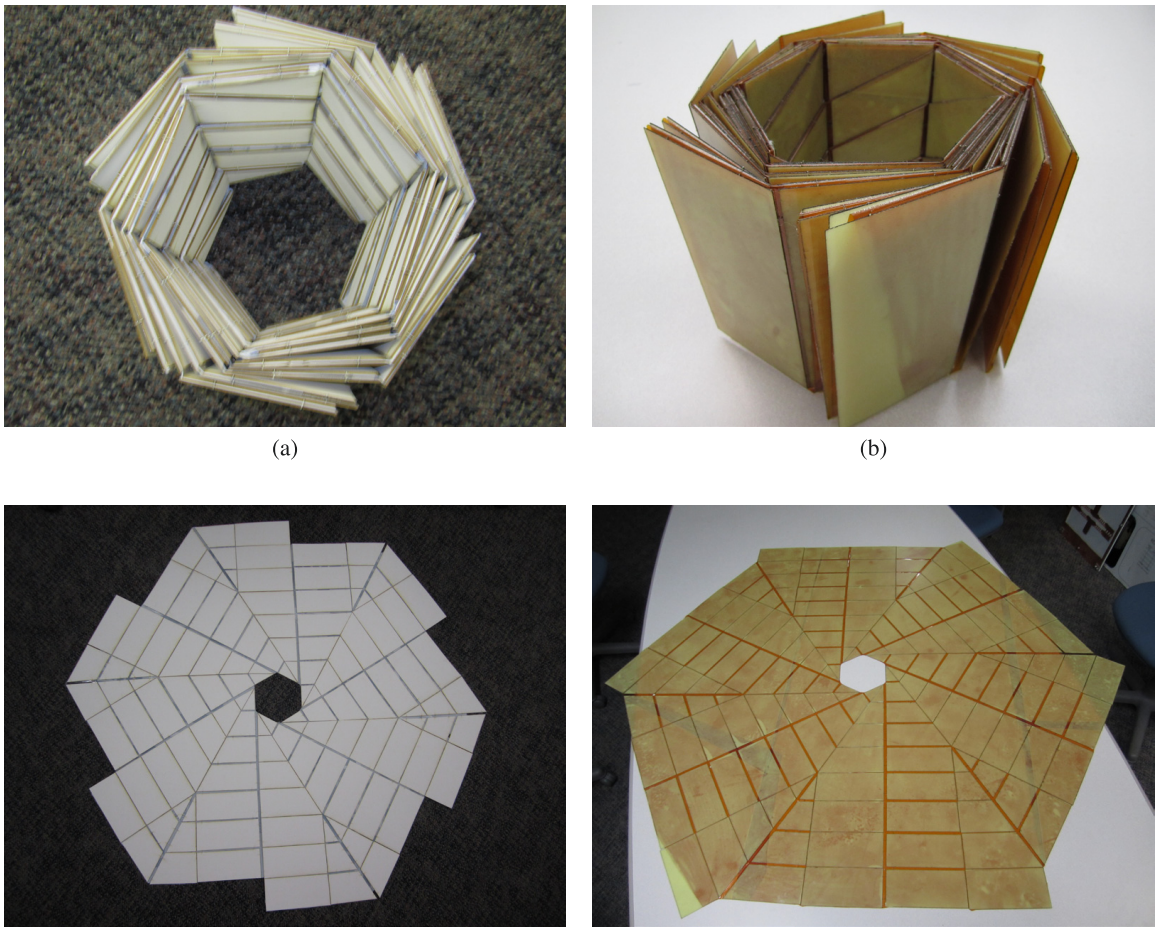

**FIGURE 11**. 1/20th scale model of the deployable hex-flasher ($m = 6$, $h = 4$, $r = 2$, and $\delta = 0.01$). Figures (a) and (c) show the model prototyped from mat board and HDPE film. Figures (b) and (d) show the model prototyped from Garolite on a Kapton film. The stowed-to-deployed diameter ratio of the model is 9.2.

division is undesirable, the alternative is to increase gap spacing between the panels. The flexing that would occur along the diagonal is now concentrated in the membrane at the gaps. With both models, an external structure is currently required to keep the deployed structure in a planar configuration. Possible future solutions include an integrated "skeletal" truss to support the panels internally, or a perimeter truss to hold the array in tension in its deployed configuration.

Actuation of the model is another important area of research. One possible solution is to embed the actuation in the model itself, perhaps through stored strain energy in deflected members or shape memory alloys (SMAs). The deployment can be guided from the outer circumference of the model with a perimeter truss. Stowing the model is slightly more challenging; the folds could be constrained to only fold in one direction (mountain or valley) from the planar state. At least six actuation points are currently needed to prevent the panels from binding on each other during the transition to the stowed state.

The membrane backing for the model can also be researched further. Preliminary testing was conducted with fabric as the membrane backing because the weave in the fabric allows shear at the membrane gaps and enables rigid foldability with smaller gap sizes. Mathematical models to quantify this motion have yet to be developed.

## ACKNOWLEDGMENT

This work was supported by a NASA Office of the Chief Technologist's Space Technology Research Fellowship and the National Science Foundation through Award No. 1240417. Part


Copyright © 2013 by ASME

of this research was carried out at the Jet Propulsion Laboratory, California Institute of Technology, under a contract with the National Aeronautics and Space Administration. Author RJL would like to acknowledge support from NSF EFRI-ODISSEI and from Jet Propulsion Laboratory for the reported work. An especial thanks to Mary Wilson and the Compliant Mechanisms Research Group at BYU for prototyping assistance.

## REFERENCES

[1] Tachi, T., 2010. "Geometric considerations for the design of rigid origami structures." *In proceedings of IASS Symposium on Spatial Structures—Permanent and Temporary*.

[2] Tachi, T., 2011. "Rigid foldable thick origami." *Origami 5: Fifth International Meeting of Origami Science, Mathematics, and Education*.

[3] Trautz, M., and Kunstler, A., 2009. "Deployable folded plate structures: folding patterns based on 4-fold-mechanism using stiff plates." *Proceedings of the International Association for Shell and Spatial Structures (IASS) Symposium*.

[4] Hoberman, C., 1991. "Reversibly expandable structures." *United States Patent No. 4,981,732*.

[5] Hoberman, C., 1993. "Curved pleated sheet structures." *United States Patent No. 5,234,727*.

[6] Hoberman, C., 2010. "Folding structures made of thick hinged sheets." *United States Patent No. 7,794,019*.

[7] Faist, K. A., and Wiens, G. J., 2010. "Parametric study on the use of Hoberman mechanisms for reconfigurable antenna and solar arrays." *In Proceedings of IEEE Aerospace Conference*, paper #1172.

[8] Miura, K., 1980. "Method of packaging and deployment of large membranes in space." *Proceedings of 31st Cong. Int. Astronaut. Federation*, pp. 1–10.

[9] Miura, K., and Natori, M., 1985. "2-D array experiment on board a space flyer unit." *Space Solar Power Review,* **5**(4), pp. 345–356.

[10] Sternberg, S., 2010. "Symmetry issues in collapsible origami." *Symmetry: Culture and Science,* **21**(4), pp. 345–364.

[11] Guest, S., and Pellegrino, S., 1992. "Inextensional wrapping of flat membranes." *Proceedings of the First International Seminar on Structural Morphology*, pp. 203–215.

[12] Nojima, T., 2002. "Origami modeling of functional structures based on organic patterns." Master's thesis, Graduate School of Kyoto University, Kyoto, Japan.

[13] De Focatiis, D. S., and Guest, S., 2002. "Deployable membranes designed from folding tree leaves." *Phil. Trans. R. Soc. Lond. A,* **360**, pp. 227–238.

[14] Lang, R. J., 1997. *Origami in Action*. St. Martin's Griffin.

[15] Shafer, J., 2001. *Origami to Astonish and Amuse*. St. Martin's Griffin.

[16] Shafer, J., 2010. *Origami Ooh La La! Action Origami for Performance and Play*. CreateSpace Independent Publishing Platform.

[17] Chiang, C. H., 1984. "On the classification of spherical four-bar linkages." *Mech Mach Theory,* **19**, pp. 283–287.

[18] Lang, R. J., 2012. "Mathematica 8 notebook." *http://www.langorigami.com/science/computational/eyeglass_flashers/eyeglass_flasher_13_ma8.nb*.

[19] NASA Technology Roadmaps, April 2012. "TA12: 2.1.3 Flexible Material Systems." *http://www.nasa.gov/pdf/501625main_TA12-ID_rev6_NRC-wTASR.pdf*.

[20] NASA Research Announcement NNL12A3001N, 2011. "Game changing opportunities in technology development." *http://prod.nais.nasa.gov/cgi-bin/eps/synopsis.cgi?acqid=152634*.

[21] NASA, 2012. "International space station: Facts and figures." *http://www.nasa.gov/mission_pages/ station/main/onthestation/facts_and_figures.htmlmain/onthestation/fact* December.



Copyright © 2013 by ASME